MISSIONE 4
ISTRUZIONE RICERCA

ITINERIS

D4.12.3: Methodologies for identification and characterization of natural and anthropogenic aerosol sources based on online measurements [B18]

Finanziato dall'Unione europea NextGenerationEU
Ministero dell'Università e della Ricerca
Italiadomani PIANO NAZIONALE DI RIPRESA E RESILIENZA

Deliverable number:	D4.12.3
Work package:	WP4 – Atmosphere
Intermediate Objective:	IO4.7
Deliverable type:	X Document, report
	☐ Websites, patent filings, videos, etc.
	☐ Other: please specify .....
Dissemination level:	X Public
	☐ Restricted
Estimated delivery (bimester):	B18
Actual delivery date:	31/10/2025
Author(s) (Partner-OU):	Daniele Contini, Daniela Cesari, Adelaide Dinoi, Fabio Massimo Grasso, Antonio Pennetta, Ermelinda Bloise, Paola Semeraro, Florin Unga, Serena Potì, Giuseppe Deluca, Luca Cirillo Ciricugno, Pierina Ielpo, Caterina Mapelli, Francesca Barnaba (CNR-ISAC)
Reviewed by:	Massimo Chiari (INFN Firenze)
Note:	

IR0000032 – ITINERIS, Italian Integrated Environmental Research Infrastructures System - CUP B53C22002150006 (D.D. n. 130/2022)
Funded by EU - Next Generation EU
Mission 4 “Education and Research” - Component 2: “From research to business” -
Investment 3.1: “Fund for the realisation of an integrated system of research and innovation infrastructures”

Table of contents

Index of Tables

Index of Figures

INTRODUCTION

This deliverable is prepared in the context of the ITINERIS project, within the Work Package 4 that deals with the integration of Research Infrastructures working in the atmospheric domain through synergistic approaches and cross boundaries developments. The deliverable reports the progress in the source identification and characterization by using online instruments for detection of aerosol composition or aerosol absorption within the Activity 4.12). Specifically, it will be discussed: the use of real-time measurements of absorption and total carbon to evaluate the brown carbon absorption and the secondary organic carbon; some results of source identification for organics using the TOF-ACSM; some examples of identification of source by using on-line ED-XRF measurements.

This document is structured in five different chapters: the introduction; three chapters dealing with the above-mentioned aspects; conclusions.

IDENTIFICATION OF CARBON SOURCES USING ONLINE DATA

Carbonaceous aerosols (CA) represent an atmospheric pollutant with critical local, regional, and global importance. CAs can be described by numerous components of different origins. According with the literature, these fractions are commonly indicated by this acronym (Massabò et al., 2021). In the following we reported a brief list of CA acronyms considered in this report:

- TC (Total Carbon) is the total mass of carbon in an aerosol sample. Frequently, TC is measured by thermal evolution or thermo-optical analysis.
- EC (Elemental Carbon) is operationally defined as the fraction of TC carbon which does not volatilize at low temperature, usually below 550°C. EC is a primary pollutant being mainly released in particle-phase from incomplete combustion processes of carbon-containing fuels.
- OC (Organic Carbon) is the fraction of TC containing organic molecules. OC includes thousands of different organic compounds (e.g., aliphatic, aromatic hydrocarbons, carboxylic acids and carboxylic compounds with polar substituent, etc.) with widely varying chemical and physical properties. It can be directly emitted as a primary OC (POC) from many sources including combustion, industrial emissions, geological and natural sources. OC can also form in the atmosphere as secondary OC (SOC), when some volatile and semi-volatile organic compounds are chemically transformed, and the products undergo condensation or nucleation.
- eBC (equivalent Black Carbon) is also defined as the TC fraction which shows a high absorption across a wide spectrum of visible and infrared wavelengths. The acronym eBC is frequently used to identify the results of optical determination of the carbon content in the PM. Many authors suggested that eBC values should be delivered together with a suitable MAC (Mass Absorption Cross-section) for the conversion of light absorption coefficient into mass concentration.

CA has a role in different atmospheric processes such as: radiative forcing (Bond et al., 2013; IPCC, 2021), heterogeneous reactions, cloud formation, and regional visibility degradation, along with their potential adverse impact on human health (Daellenbach et al., 2020; Tomašek et al., 2021; WHO, 2021). The carbonaceous fraction is an important component of PM, generally representing between 20% and 50% of its mass (Kanakidou et al., 2005; Putaud et al., 2010), mainly of anthropogenic origin (Bond and Bergstrom, 2006) and because of its effects, scientific community has increased his attention in this pollutant. An intensive observation campaign has been performed between March and April 2023, collecting in parallel daily samples of PM10 and PM2.5 and measuring on these samples OC and EC concentrations. Simultaneously, equivalent black carbon (eBC) concentrations were monitored online by means of three different instruments: a Multi-Angle Absorption Photometer (MAAP), an aethalometer (AE33), and a Giano BC1 black carbon analyser.

Measurement site and set-up

The sampling site is at institute CNR-ISAC of Lecce, where is located the Environmental Climate Observatory (named in the following ECO) (SE Italy, 40°20’8” N - 18°07’28” E, 37 m a.s.l.) (Fig. 1a). The study site, classified as an urban background site (Cesari et al., 2018), is subjected to long-range transport phenomena from East Europe and coarse dust advection events from Africa, as well as sea spray contribution and secondary aerosol formation due to photochemical transformation of air pollutants, thus representing a mix of regional background conditions in the heart of the Mediterranean basin. The sampling set-up used for this study was composed of two automatic aerosol sampler: the SWAM 5A Dual Channel Monitor (FAI Instruments srl), located in the ECO shelter (Figure 1a), providing simultaneously PM_{10} and $PM_{2.5}$ mass concentrations according to the ß-attenuation method; and the Giano BC1 black carbon analyser, composed of a standard low-volume PM sampler equipped with an optical module for eBC online measurements. The Giano BC1 was

installed on the roof of the ISAC building, close to the ECO shelter (Figure 1b). In this report, the PM concentrations used for data analysis are those measured with the SWAM5A Dual Channel Monitor. Between 22 March and 19 April 2023, 86 aerosol samples (57 PM_{10} and 29 $PM_{2.5}$) were collected, using quartz fibre filters (Whatmann, 47 mm in diameter). All filters were thermally pre-treated (for 2h at 700°C) to remove, before sampling, any residual carbon contamination on blank membranes (Dinoi et al., 2017). The collected daily PM samples were stored at 4°C between until the EC/OC analysis. The analysis of carbonaceous species (i.e. EC/OC) in PM samples were done using a Sunset OC/EC Analyser (Sunset Laboratory Inc., OR, USA, Figure 1b) operating with the EUSAAR2 protocol (thermo-optical method). A multipoint calibration, using as external standard a sucrose solution (2.198 g/l in water, CPAchem Ltd), was done to correct OC and EC measured concentrations. Linear calibration had a slope of 0.97, a negligible intercept, and a determination coefficient R^2=1.

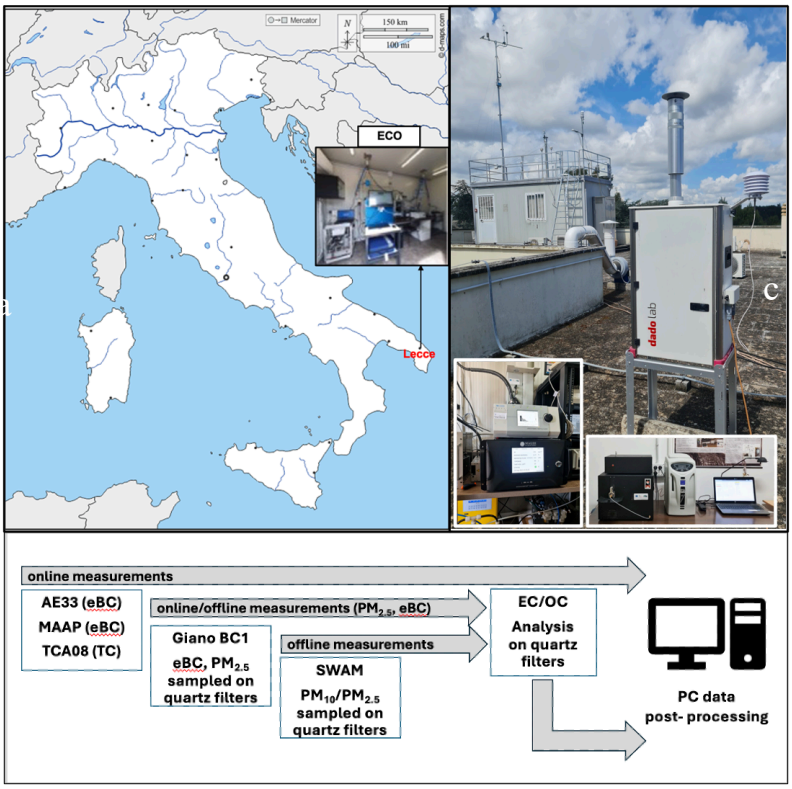

Figure 1. Sampling set-up: the ECO facility and the Giano BC1 black carbon analyser.

In measurements of eBC, the Mass Absorption Cross-section (MAC) is an important parameter to describe the optical properties of EC (Liu et al., 2015). MAC has been firstly introduced by Bond et al. (2006) as the light absorption cross section normalized to the mass of a given species (e.g. BC) of aerosol particles (in units of m^2/g) both for absorption or scattering cross section, and is applied for the conversion of the light absorption coefficient to eBC mass concentration. In this work the MAC values determined in-situ and reported in a previous deliverable and in Cesari et al (2025) are used.

Further information regarding carbonaceous aerosol have been gained by a Real Time Total Carbon Aerosol Analyzer (Aerosol Magee Scientific, TCA08) located in the ECO observatory. This instrument, equipped with a $PM_{2.5}$ head, uses a thermal method for TC determination. It is composed of two parallel flow channels with two analytical chambers, which alternate between sample

collection and thermal analysis, giving a semi-continuous TC measurement. Further, it is possible obtain the concentration of organic carbon (OC) by subtracting black carbon concentration measured by the AE33, from the total carbon concentration measured by the TCA08.

Determination of hourly POC and SOC from TCA data

Data collected with the TCA08 analyser allowed the determination of the secondary organic carbon (SOC) and of the primary organic carbon (POC), following the method described in Ivančič et al., (2022) and assuming that POC and BC are co-emitted by combustion sources. The equations are:

$$POC=(OC/BC)_{prim} \times BC \qquad \text{(Eq. 4)}$$

$$SOC=OC - POC \qquad \text{(Eq. 5)}$$

For calculating the ratio $(OC/BC)_{prim}$, the R-squared method has been used. Briefly, the hypothetical SOC is firstly calculated for a wide range of hypothetical $(OC/BC)_{prim}$ ratios (for ratios 0.1 to 10 in 0.1 steps). SOC and BC is calculated for every hypothetical $(OC/BC)_{prim}$ ratio, and the optimal $(OC/BC)_{prim}$ ratio is chosen where the R-squared is minimal. In Figure 2 a summary of PM_{10} and $PM_{2.5}$ measurements together with OC/EC thermo-optic determination is reported for the studied period.

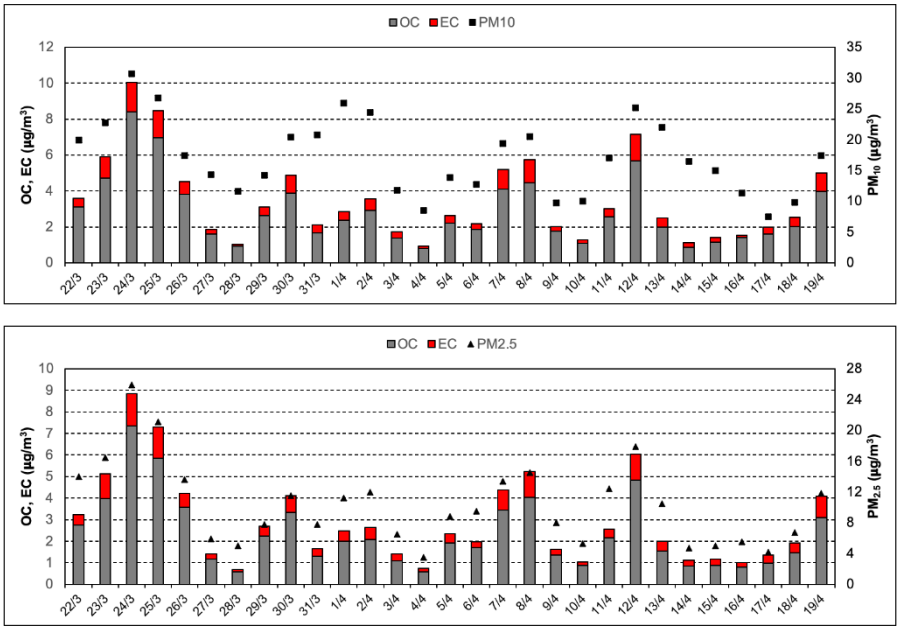

Figure 2. Daily trend of OC and EC both in PM10 (top) and PM2.5 (bottom) fractions.

The average concentrations of PM obtained were 17.1 (± 1.1) µgm^3 for PM_{10} and 10.4 (± 1.0) µg/m^3 for $PM_{2.5}$. Considering the whole measurement period, OC and EC represented, on average, 16.5% and 3.6 % of PM_{10} in mass, and 22.6% and 5.5% of $PM_{2.5}$. These values are in agreement with those reported in a recent study of Merico et al., (2025). The complete dataset of eBC raw data, collected with MAAP, AE33 and Giano BC1, and EC concentration, obtained with the Sunset (EUSAAR2 protocol), were used to estimate the MAC in-situ. In Table 1, the new values of MAC are reported.

In Figure 3 the daily pattern of eBC, measured with MAAP, AE33 and GIANO BC1, is reported. The daily pattern shows some interesting aspects. The first is that the lowest concentrations are observed around midday and early afternoon and there is a clear modulation of the atmospheric eBC concentrations due to the daily evolution of the planetary boundary layer (PBL) height. The second aspect is that in the early morning a peak is evident, probably due to traffic emissions, which occurs

at 6 am. Finally, during the evening/nighttime there is a eBC peak higher that is probably due to a mixed effect between the PBL dynamics and the traffic and domestic heating emissions.

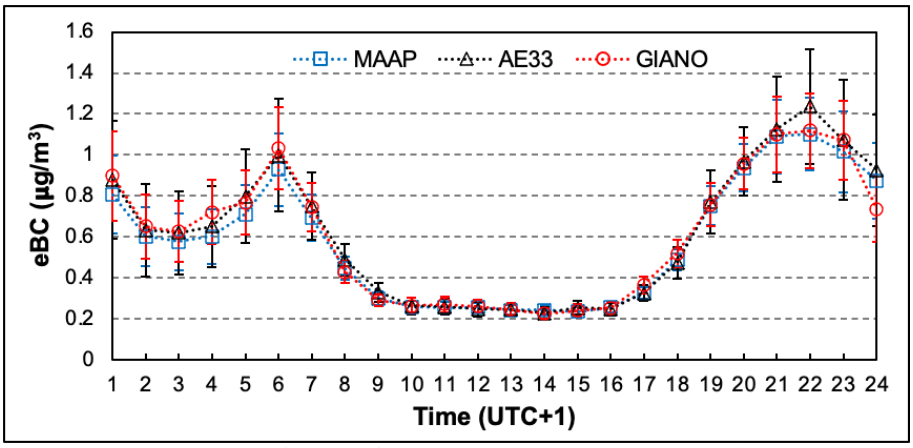

Figure 3. Daily pattern of eBC (µg/m3) measured with MAAP, AE33 and GIANO BC1.

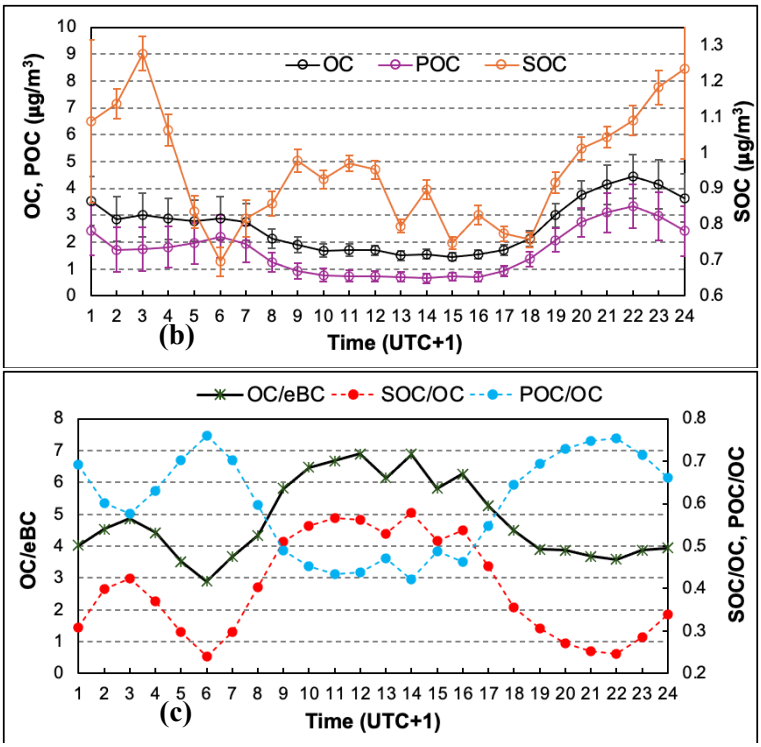

Figure 4. Daily pattern of OC, SOC and POC (µg/m3) obtained by measurement from with TCA. Daily pattern of eBCff and eBCbb retrieved with Aethalometer model approach.

In Figure 4 the daily patterns of OC, POC, and SOC are shown togheter with some diagnostic concentration ratios. In Figure 5 the biomass burning contribution to eBC measured with AE33 is reported together with the fossil fuel contribution. As already mentioned, multi-wavelength Aethalometer data may be used to derive the fossil fuel and the biomass burning contributions to eBC (eBC_{ff} and eBC_{bb}, respectively). This approach is called "Aethalometer model" and assumes that light-absorbing particles only originate from vehicle and biomass-burning emissions (Sandradewi et al., 2008; Zotter et al., 2017). Results showed that, on average, eBC_{ff} accounted for about 65% of the measured eBC, while the eBCbb is only 35%, indicating that the ECO site is more influenced by fossil fuel combustion in spring season. The analysis of the daily pattern showed two pronounced peaks for eBC_{ff}: the former in the early morning at 6 a.m., the second in the evening at 22 p.m., clearly associated with human activity, traffic emissions in particular. As previously stated, the nighttime peak could be due to a combined effect of traffic emissions and the PBL height. Regarding the eBC_{bb} daily patter, this is mainly characterized by a peak during the evening/night, less pronounced than that of eBC_{ff}, that could be due both to the use of biomass burning for domestic heating and a to the PBL dynamic.

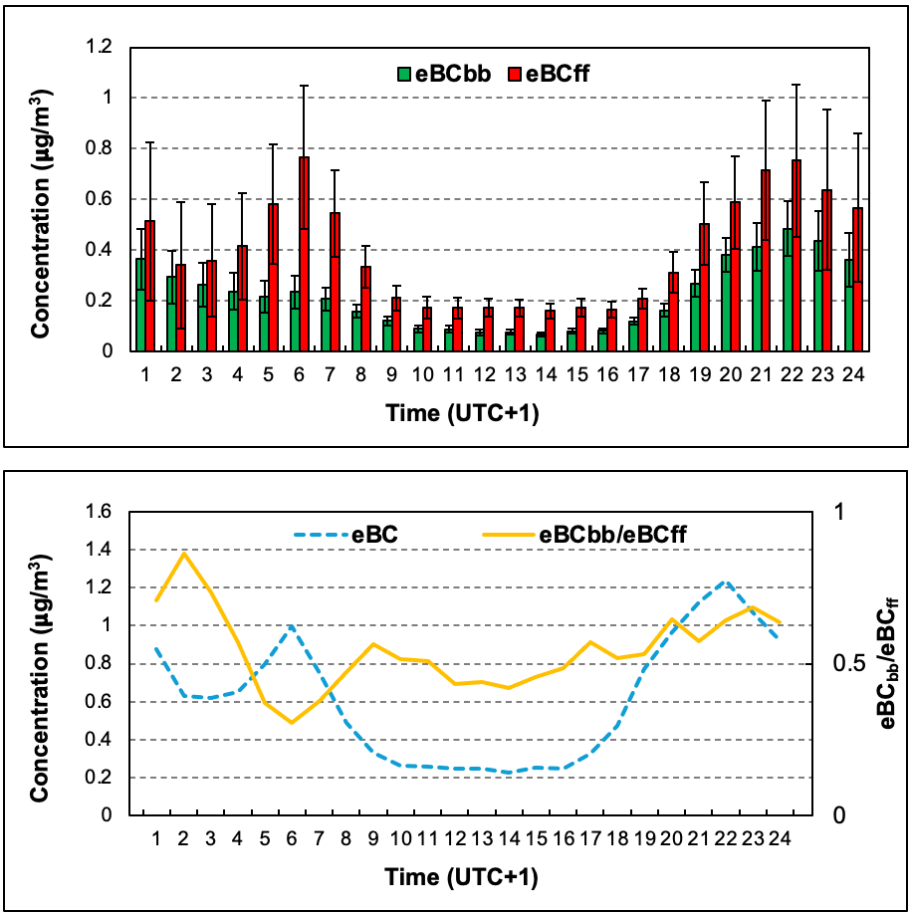

Figure 5. Daily pattern of eBCff and eBCbb retrieved with Aethalometer model approach.

The average AAE calculated for aerosols collected at the ECO site was 1.46, suggesting the presence of brown carbon (BrC). It is important to highlight that the reported AAE value is an average estimates that may vary under real atmospheric conditions, being site-dependent and can vary significantly due to factors such as PM source contributions, atmospheric processing, and the evolving properties of carbonaceous aerosol, including morphology, size distribution, aging, transport, and microphysical characteristics. Distinguishing between black carbon and brown carbon

solely based on AAE may not be quantitatively precise, as auxiliary measurements providing information on particle size, coating thickness, chemical composition, and particle morphology are necessary to support accurate aerosol characterization. However, despite these uncertainties, determining the AAE remains crucial for understanding the optical properties of different aerosol types. Accordingly, the results presented in this study should be interpreted as indicative of the presence and relative contribution of BrC, rather than as exact quantitative values. In Figure 6 the absorption coefficients (babs) are reported as a function of wavelength in the investigated range 370 nm - 950 nm. The red line represents the total absorption given by AE33 for the aerosol collected in ECO site (AAE=1.46), while black line represent absorption by eBC (AAE=1) with the grey-shaded area indicating the eBC absolute contribution. The orange-shaded area represents the BrC contribution, calculated as the difference between the total AE33 absorption and the estimated eBC absorption.

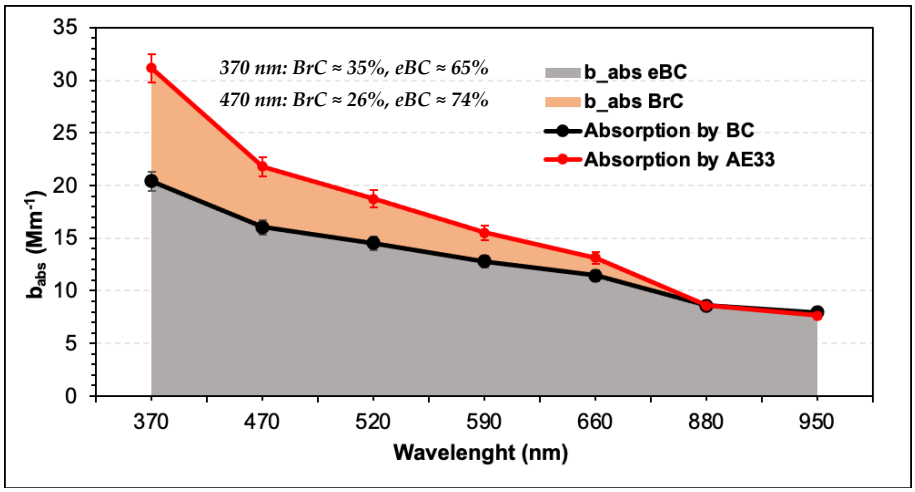

Figure 6. Wavelength dependence of average absorption coefficients (babs) and relative contribution of eBC and BrC to the total absorbance measured with AE33. The relative contributions of BrC and eBC are explicitly annotated at the key wavelengths (370

Summary

- An intensive observatory campaign has been performed between March and April 2023, collecting in parallel daily samples of PM_{10} and $PM_{2.5}$, determining their content in OC and EC concentrations and simultaneously, collecting in high time resolution eBC and TC data.
- The average concentrations of PM obtained were 17.1 (± 1.1) µgm^3 for PM_{10} and 10.4 (± 1.0) µgm^3 for $PM_{2.5}$. Considering the whole measurement period, OC and EC represented, on average, 16.5% and 3.6 % of PM_{10} in mass, and 22.6% and 5.5% of $PM_{2.5}$.
- The diurnal variations in eBC and POC concentrations highlighted the strong influence of local sources at ECO site, i.e. traffic (contributing to the eBC for 64%) and biomass burning for residential heating (contributing to the eBC for 36%), modulated by local meteorological dynamics. The application of the Aethalometer model showed that fossil fuel combustion was the dominant source of eBC at ECO site, though biomass burning also played a relevant role, especially during evening and early morning hours. SOC contributions, accounting for 36% of the measured OC, were more prominent during midday hours, reflecting the enhanced photochemical activity in this part of the day.
- The analysis of the aerosol optical properties performed with AE33 indicated the presence of a certain amount of BrC in the collected aerosol, particularly at shorter wavelengths (up to 35% of absorption at 370 nm). The BrC_{abs} diurnal pattern at 370 nm was higher during the

night-time and decreasing in the diurnal hours, suggesting that this parameter was mainly influenced by biomass burning source (or domestic heating) at ECO site.

- The use of on-line measurements of total carbon coupled with aethalometer measurements allows the high temporal resolution apportionment of eBC, the determination of primary and secondary OC, and the estimate of the absorption due to brown carbon.

IDENTIFICATION OF SOURCES BY MEANS OF THE TOF-ACSM

The Aerosol Chemical Speciation Monitor TOF-ACSM089 was installed in the new shelter of ECO station in September 2024. Here the preliminary data analysis of the period 24/09/2024-17/02/2025 is reported. The instrument can furnish measurements at high temporal resolution (10 minutes) of some chemical components of PM_1 and it could furnish information useful for near-real-time source apportionment and for source identification. Specifically, the results reported here are:

- temporal variability of measurements for the period 24/09/2024 – 17/02/2025
- a first comparison of ToF-ACSM with SMPS data
- a first determination of the detection limits in current operative conditions
- Source apportionment of organics using the software Sofi Pro

Further development will include the post-processing of the data collected after 27/05/2025.

The acquired data were validated according to the methodology reported in the Tofware user guide for Tof ACSM manual (updated July 2023 – Aerodyne). Figure 7 shows the time series in UTC of the data for the following species: Organics (Org), nitrate (NO_3), sulphate (SO_4), ammonium (NH_4) and chloride (Chl). Starting from the end of November 2024, an increase in the concentration of organic matter is observed (mean and standard error of the period 24/09/2024 – 8/11/2024: 4.8 ± 0.1 µg/m^3; mean and standard error of the period 16/11/2024 – 17/02/2025: 7.9 ± 0.2 µg/m^3), an increase in nitrate concentrations (mean and standard error of the period 24/09/2024 – 8/11/2024: 0.69 ± 0.02 µg/m^3; mean and standard error of the period 16/11/2024 – 17/02/2025: 1.16 ± 0.03 µg/m^3) and a decrease in sulphate concentrations (mean and standard error of the period 24/09/2024 – 8/11/2024: 1.68 ± 0.03 µg/m^3; mean and standard error of the period 16/11/2024 – 17/02/2025: 0.84 ± 0.01 µg/m^3).

Figures 8 shows the daily patterns of the different measured components. It is observed that organics have a daily pattern comparable to that of OC with lower values during diurnal hours. The same applies for nitrate, while sulphate and ammonium have limited daily variabilities. Figure 9 shows weekly patterns of the different chemical species.

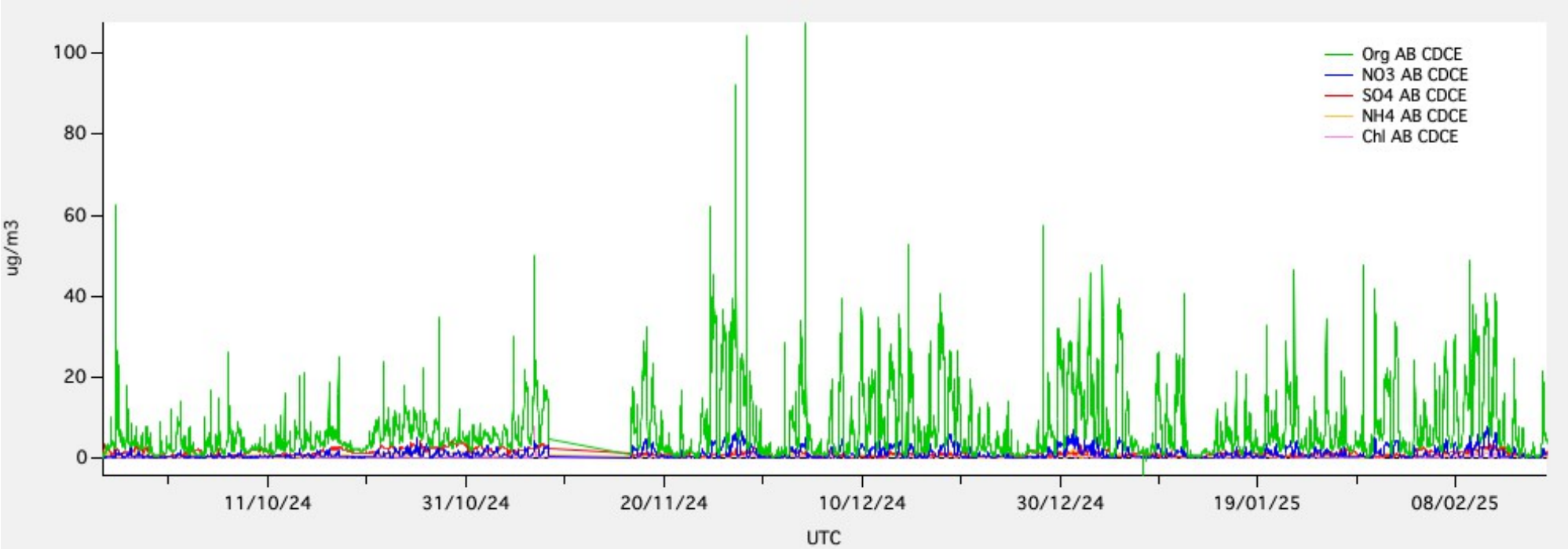

Figure 7. Time series in UTC for the different species. In the legend, the corrections made to the raw data are indicated next to the species: AB indicates the correction for the air beam, while CDCE indicates the one related to the Composition Dependent

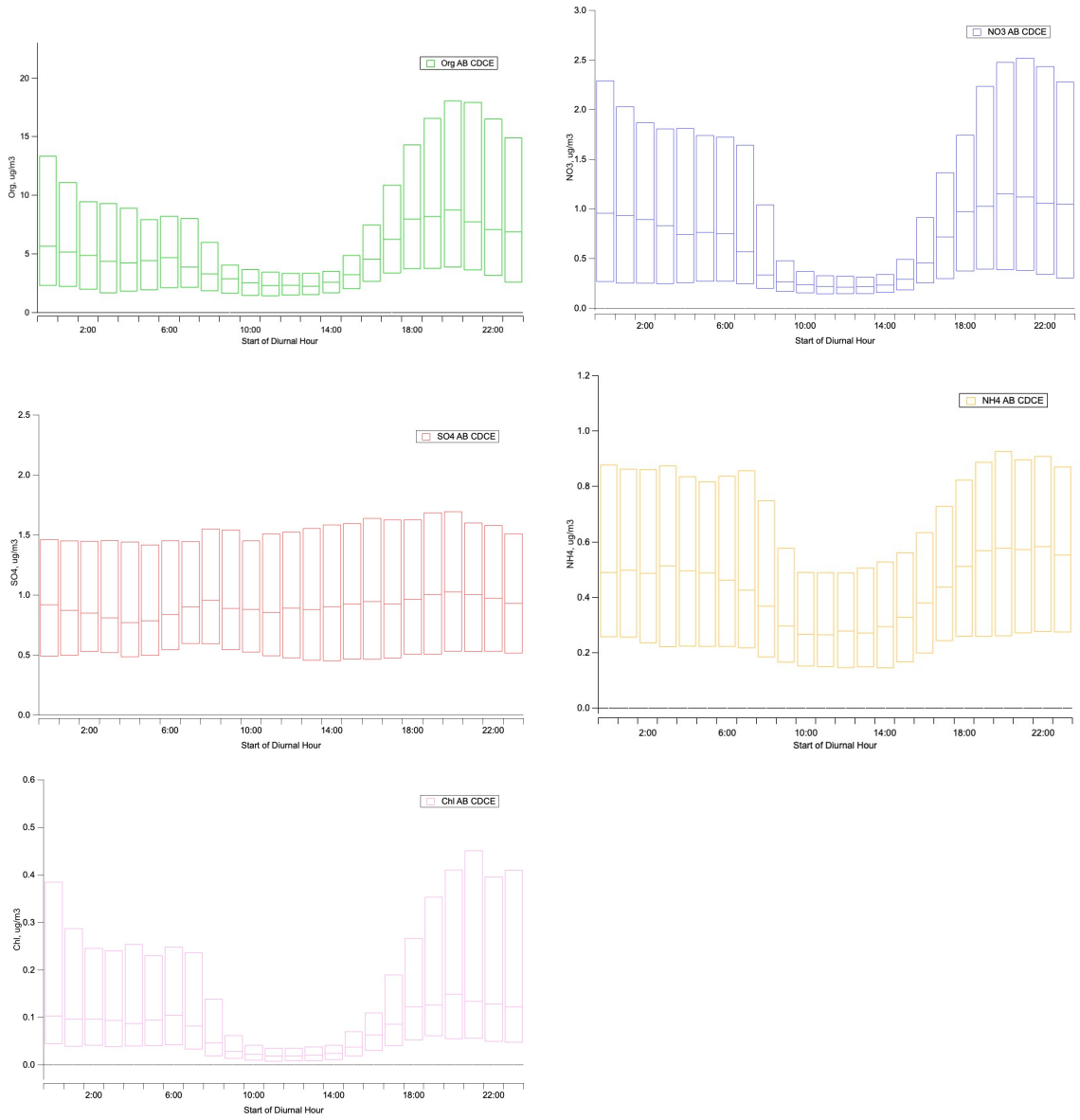

Figure 8. Daily patterns of the different chemical species. Time in UTC.

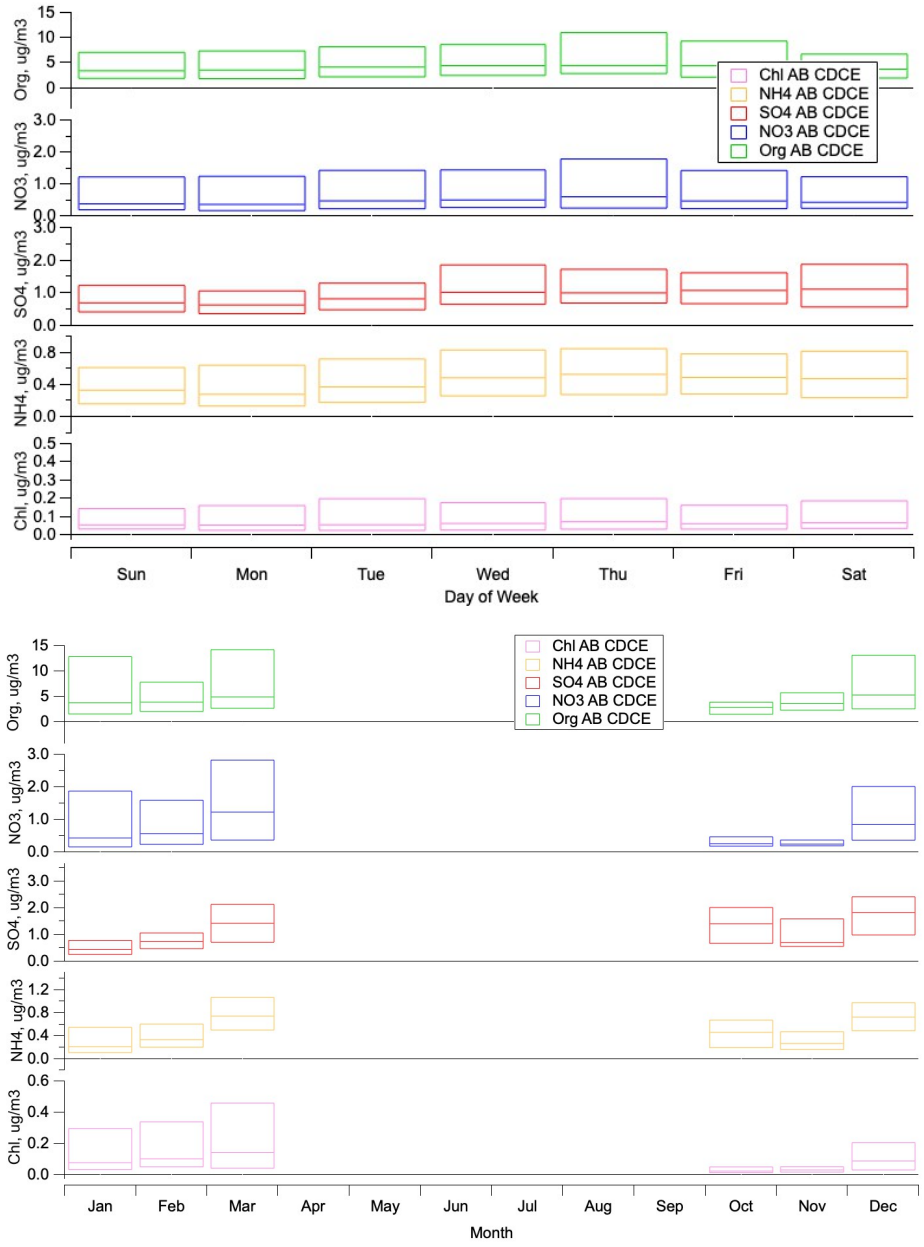

Figure 9. Weekly and monthly patterns of the different chemical species.

As reported in the COST Action COLOSSAL guidelines (2019), in order to evaluate the accuracy of the tuning and calibration parameters of the ToF-ACSM operating conditions, it is necessary to compare the data obtained from ACSM measurements with external data from co-located measurements, obtained on the same size fraction. In general, the comparison is based on the concept of reconstructing PM concentrations as the sum of the concentrations of the major species, i.e.,

$PM1_{,\,chem} = NO_3 + SO_4 + NH_4 + Cl + Org + eBC$

where NO_3, SO_4, NH_4, Cl, Org are the concentrations of nitrate, sulphate, ammonium, chloride, and organic aerosol measured by the ACSM (after data post-processing) and eBC are the concentrations of black carbon derived from photometric absorption measurements.

The $PM1_{,\,chem}$ values can therefore be compared with external PM data obtained from co-located measurements. Figure 10 compares the hourly mean PM1 volume concentrations obtained from the ACSM ToF with those obtained from the SMPS from September 24, 2024, to January 29, 2025.

The hourly mean mass concentrations obtained from the ACSM ToF data were converted to volume concentrations by dividing the mass concentrations of each species by their respective densities, then summed together and finally compared with the corresponding volume concentrations obtained from the SMPS (COST Action COLOSSAL (2019)). As shown, there is good correlation between the ACSM ToF data and the SMPS data ($R^2 > 0.80$; COST Action COLOSSAL (2019)), however the slope is significantly larger than one and this should be furtherly investigated and it could be partly due to the eBC values that were not considered in the comparison as they were not available for the PM1 fraction.

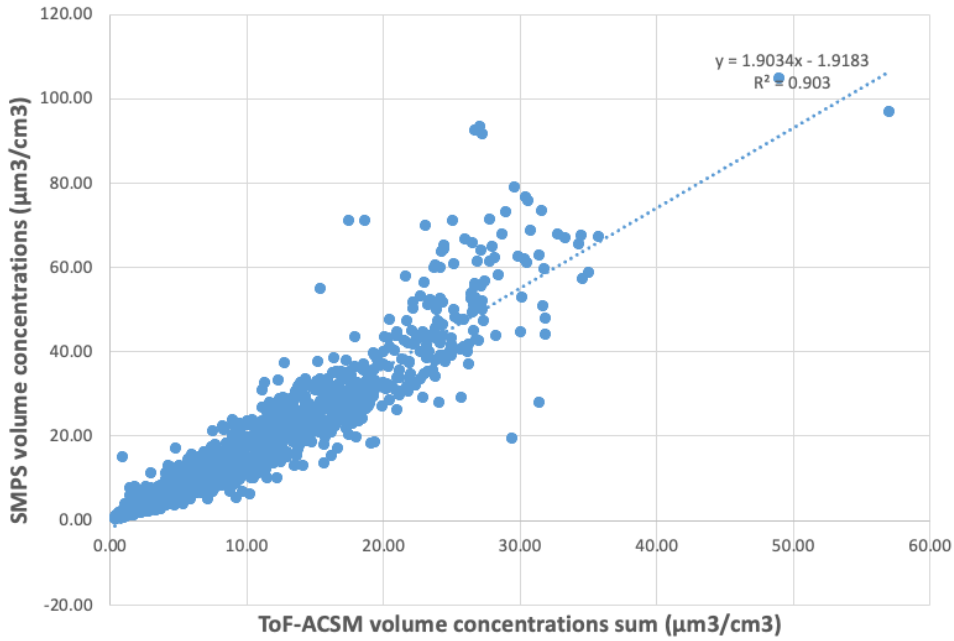

Figure 10. Comparison of PM1 reconstructed by TOF-ACMS with the values obtained by the SMPS.

After replacing the diaphragms of the ACSM ToF forepump, and before restarting continuous acquisition, the ammonium detection limit was determined by placing an EPA filter upstream of the sampling line (see Figure 11). The detection limit in question, obtained as 3 times the standard deviation of the concentrations, was estimated on an acquisition dataset spanning over 12 hours (6:44

PM on May 26, 2025 – 7:44 AM on May 27, 2025) and is equal to 0.28 µg/m^3. This value will be used for data post-processing instead of the default value.

Figure 11. Setup with HEPA filter for TOF-ACSM.

The following are the preliminary results of source apportionment of data for the period September 24, 2024 – February 14, 2025 using Sofi Pro software. The four- and five-factor solutions are discussed.

Four-factor solution

The first factor is characterized by the contribution of oxygenated fragments with m/z 29, 60, and 73; the second and fourth factors are dominated by oxygenated fragments with m/z 43 and 44; while the third factor is characterized by contributions of hydrocarbon fragments with m/z 29, 41, 43, and 55. These factors, according to the nomenclature used in ACTRIS, are identified as:

- BBOA (biomass burning OA). The diurnal cycle of this factor shows a peak during the evening hours.
- LO-OOA (less oxidized-oxygenated OA). This factor appears to be significantly influenced by BBOA and therefore could be an oxidation product of BBOA or an SOA composed of gaseous emissions linked to BBOA and MO-OOA.
- MO-OOA (more oxidized-oxygenated OA)
- HOA (hydrocarbon-like OA). The diurnal cycle of this factor shows a bimodal trend with morning and evening peaks.

Five-factor solution

In the five-factor solutions, BBOA is split into two: one appears to be the classic BBOA associated with wood combustion for domestic heating, whose contribution increases towards the end of November and remains almost constant thereafter (figure 14: factor 5 in blue - BBOA1), the other has a more episodic nature and could be linked to agricultural biomass combustion or similar events

(figure 14: factor 1 in red - BBOA2). Adding these together yields the BBOA amount of the four-factor solution; the solutions appear to be quite consistent. To confirm this split, a comparison with tracer data sampled in the same period, such as levoglucosan, will be necessary.

Furthermore, the solutions with constrains for HOA, BBOA, and COA (cooking OA) were tested with the software used. In particular, the solutions with constrained BBOA and COA were excluded because the BBOA profile appears to be significantly different from that of the typical profile. So much so that when forced, both the forced profile and another factor are obtained, as the model cannot explain all the BBOA present in the matrix. Meanwhile, the COA (cooking OA) does not appear to be significantly present: forcing it results in a profile that does not have the expected diurnal trend and is therefore likely an artifact.

The solutions with constrained HOA show a rather modest impact on quantification, which does not justify their use for the current data set.

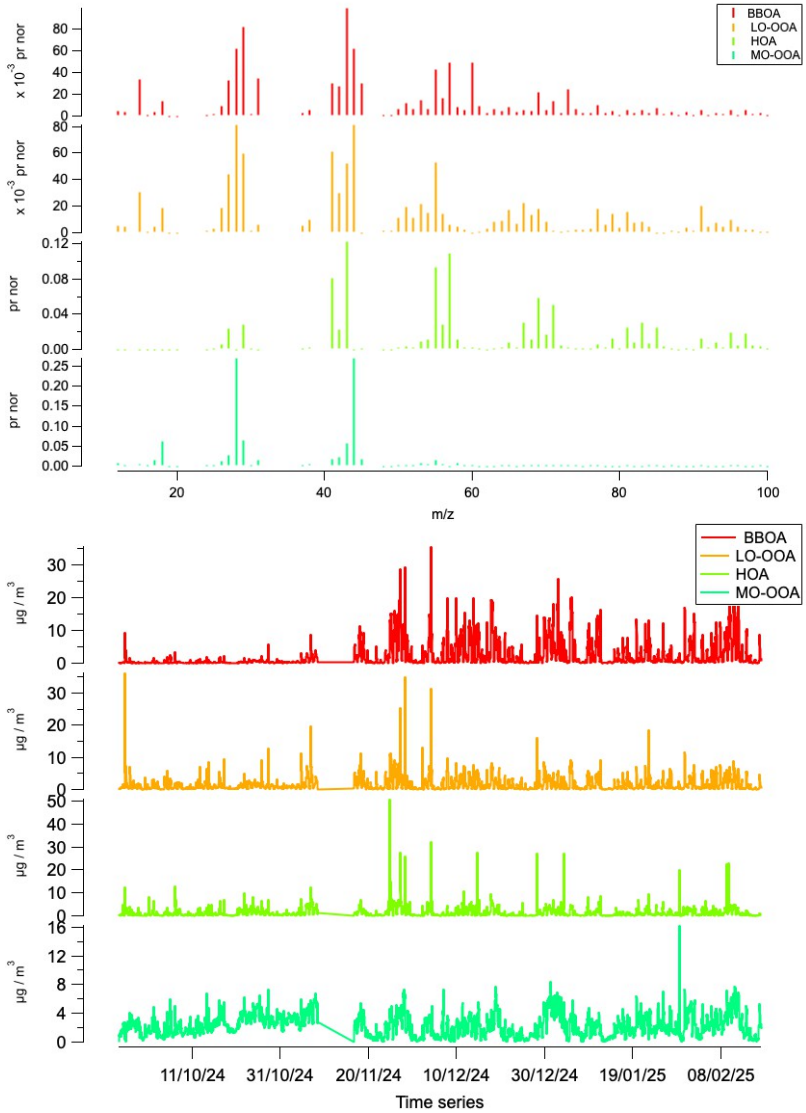

Figure 12. Factor profiles in terms of mass/charge ratio for a four-factor solution Time series (UTC) of contribution for the four-factor solution.

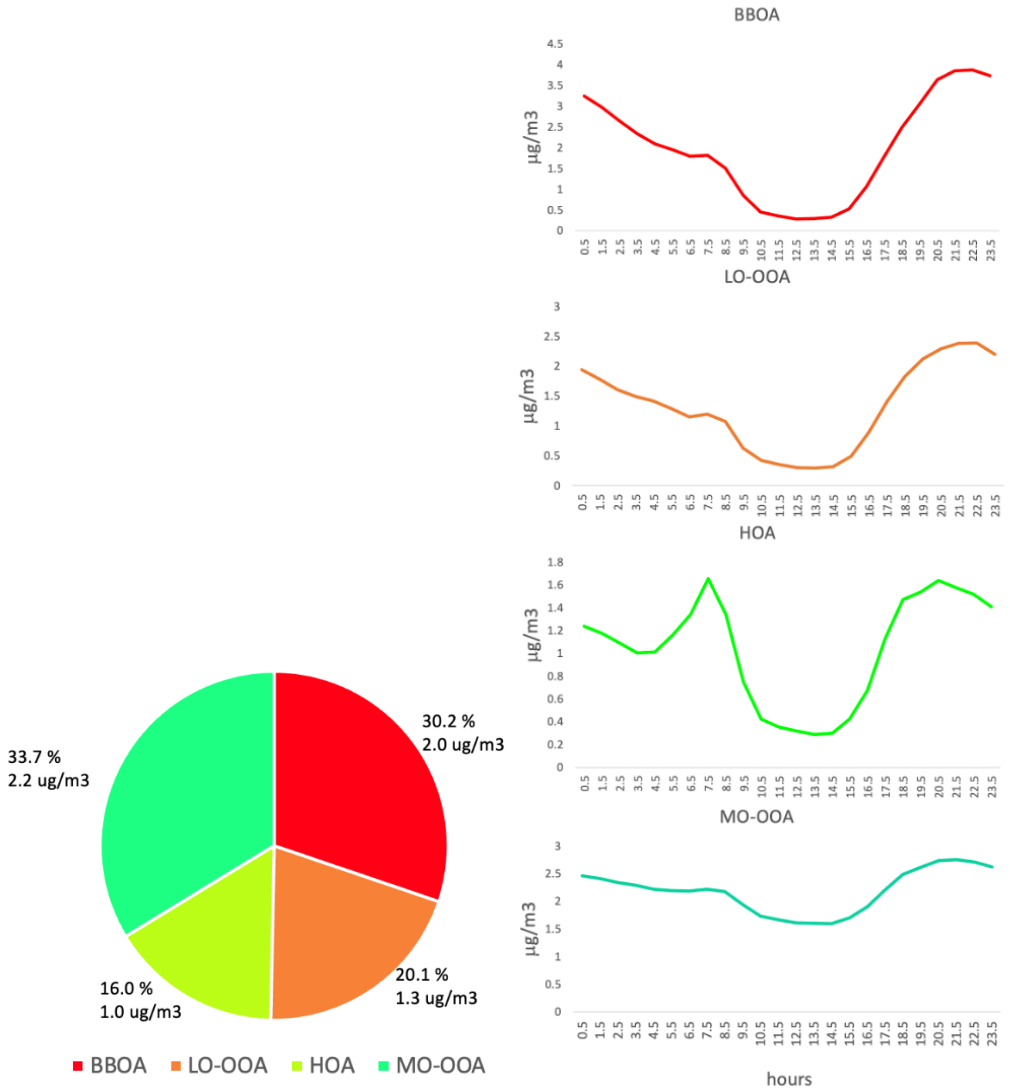

Figure 13. Pie-graph of the average contributions and daily patterns for the four-factor solution, time in UTC.

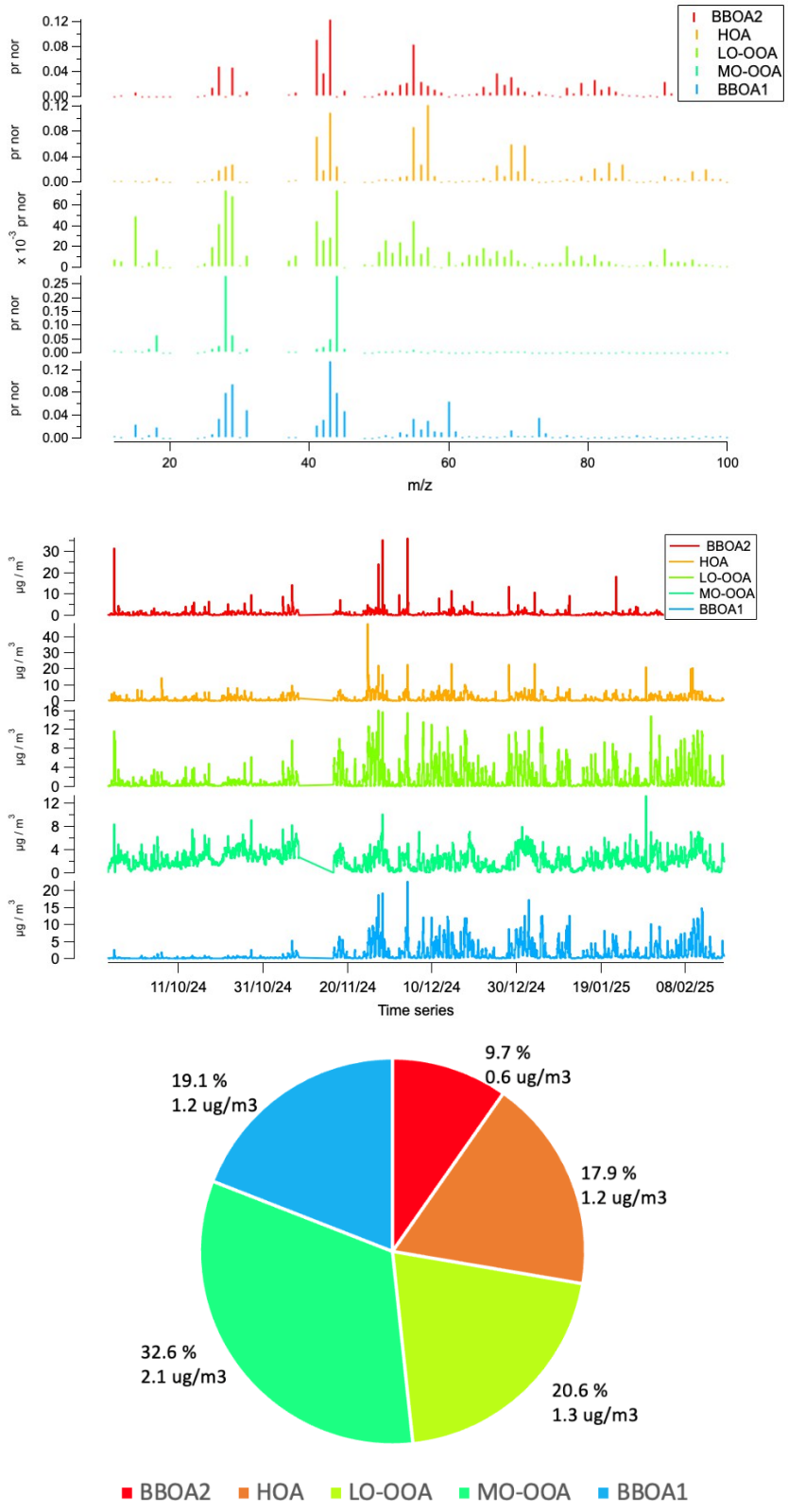

Figure 14. Factor profiles in terms of mass/charge ratio for a four-factor solution Time series (UTC) of contribution for the five-factor solution and pie-graph of average contributions.

IDENTIFICATION OF SOURCES BY MEANS OF THE ONLINE ED-XRF SYSTEM (XACT)

The Xact® 625i instrument has been installed at ECO (new shelter) for online detection of the elemental chemical composition of atmospheric PM_{10} that could provide valuable insights into the nature of its emission sources. In this context, the ECO laboratory, through the ITINERIS project, has acquired an Xact® 625i analyser, specifically designed for near real-time monitoring of metal concentrations in ambient air. This instrument offers high temporal resolution and detection limits comparable to traditional offline laboratory analyses for the majority of the elements. The Xact® 625i is equipped with a meteorological station that records wind speed and direction. Sampling is performed using a PM10 inlet with an operational flow rate of 16.7 L/min. The instrument is calibrated for 44 elements: *Al, Si, P, S, Cl, K, Ca, Ti, V, Cr, Mn, Fe, Co, Ni, Cu, Zn, Ga, Ge, As, Se, Br, Rb, Sr, Y, Zr, Mo, Pd, Ag, Cd, In, Sn, Sb, Te, Cs, Ba, La, Ce, W, Pt, Au, Hg, Tl, Pb e Bi*. A 3-hour sampling interval was chosen to enhance measurement sensitivity. Under the typical conditions of the observatory, not all calibrated species are effectively quantified above the detection limits. Below are the preliminary results from the first measurement period, spanning from 30/11/2024 to 30/06/2025. Table 2 presents the 34 measurable elements and their corresponding limit of detection (LOD) values, considering a sampling time of 3 hours, according to manufacturer. The third column indicates the percentage of measurements exceeding the LOD during the analysed period.

Elements	LOD (ng/m^3)	Data Above LOD (%)
Aluminium (Al)	19	100
Silicon (Si)	3.4	81
Sulphur (S)	0.6	100
Chlorine (Cl)	0.33	100
Potassium (K)	0.22	100
Calcium (Ca)	0.057	100
Titanium (Ti)	0.03	100
Vanadium (V)	0.023	77
Chromium (Cr)	0.022	94
Manganese (Mn)	0.027	97
Iron (Fe)	0.033	100
Cobalt (Co)	0.026	0
Nickel (Ni)	0.018	99
Copper (Cu)	0.015	100
Zinc (Zn)	0.013	100
Gallium (Ga)	0.011	21
Germanium (Ge)	0.011	0
Arsenic (As)	0.012	99
Selenium (Se)	0.016	86
Bromine (Br)	0.02	100
Strontium (Sr)	0.041	99
Molybdenum (Mo)	0.092	0
Palladium (Pd)	0.42	0
Silver (Ag)	0.37	100

Cadmium (Cd)	0.48	17
Tin (Sn)	0.78	4
Antimony (Sb)	0.99	3
Barium (Ba)	0.074	81
Lanthanum (La)	0.069	0
Platinum (Pt)	0.023	0
Mercury (Hg)	0.023	0
Thallium (Tl)	0.022	0
Lead (Pb)	0.024	84
Bismuth (Bi)	0.025	9

Table 1. List of the 34 measurable elements, their corresponding LOD values, and the percentage of measurements exceeding the LOD during the analysed period.

The UO ISAC-Lecce participated to an inter-comparison of Xact measurements organized by the Section of Firenze of INFN within the MITRAP project and the preliminary results were presented at the European Aerosol Conference EAC2025 (Fratticcioli et al., 2025). However, final results are not available yet and this will not be further discussed in this report.

An inter-comparison of Xact online measurements with benchtop off-line ED-XRF elemental concentrations was finally performed on 14 elements (Al, S, Cl, K, Ca, Ti, Cr, Mn, Fe, Cu, Zn, Br, Sr, Pb). The off-line measurements were done on quartz filters sampled independently from the tape of Xact using the calibration and correction factors defined in Dinoi et al., 2024; Unga et al., 2025). Therefore, there could be differences due to non-completely corrected matrix effects as well as to the difference in the sampling. Results, presented at the European Aerosol Conference EAC2025 (Deluca et al., 2025), are shown in Figure 14. The Figure 15(a) shows box plots of the concentrations for the elements that were compared. The bottom and the top of each box are the 25th and 75th percentiles, respectively, the line in the middle of the box is the median; the bottom and top whiskers are the minimum and maximum value respectively. The part (b) shows the coefficient of determination of the linear regression for each element.

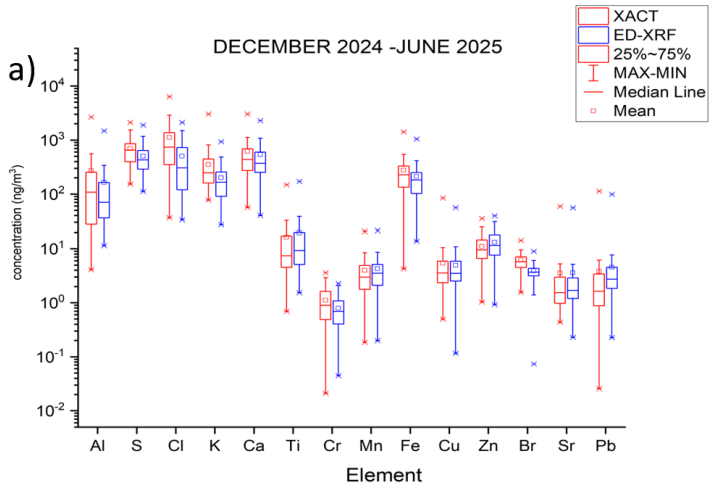

b)

ELEMENT	R^2
ALUMINIUM	0.949
SULPHUR	0.792
CHLORINE	0.695
POTASSIUM	0.715
CALCIUM	0.951
TITANIUM	0.996
CHROMIUM	0.867
MANGANESE	0.915
IRON	0.992
COPPER	0.954
ZINC	0.842
BROMINE	0.560
STRONTIUM	0.992
LEAD	0.995

Figure 15. Intercomparison of Xact and benchtop ED-XRF measurements.

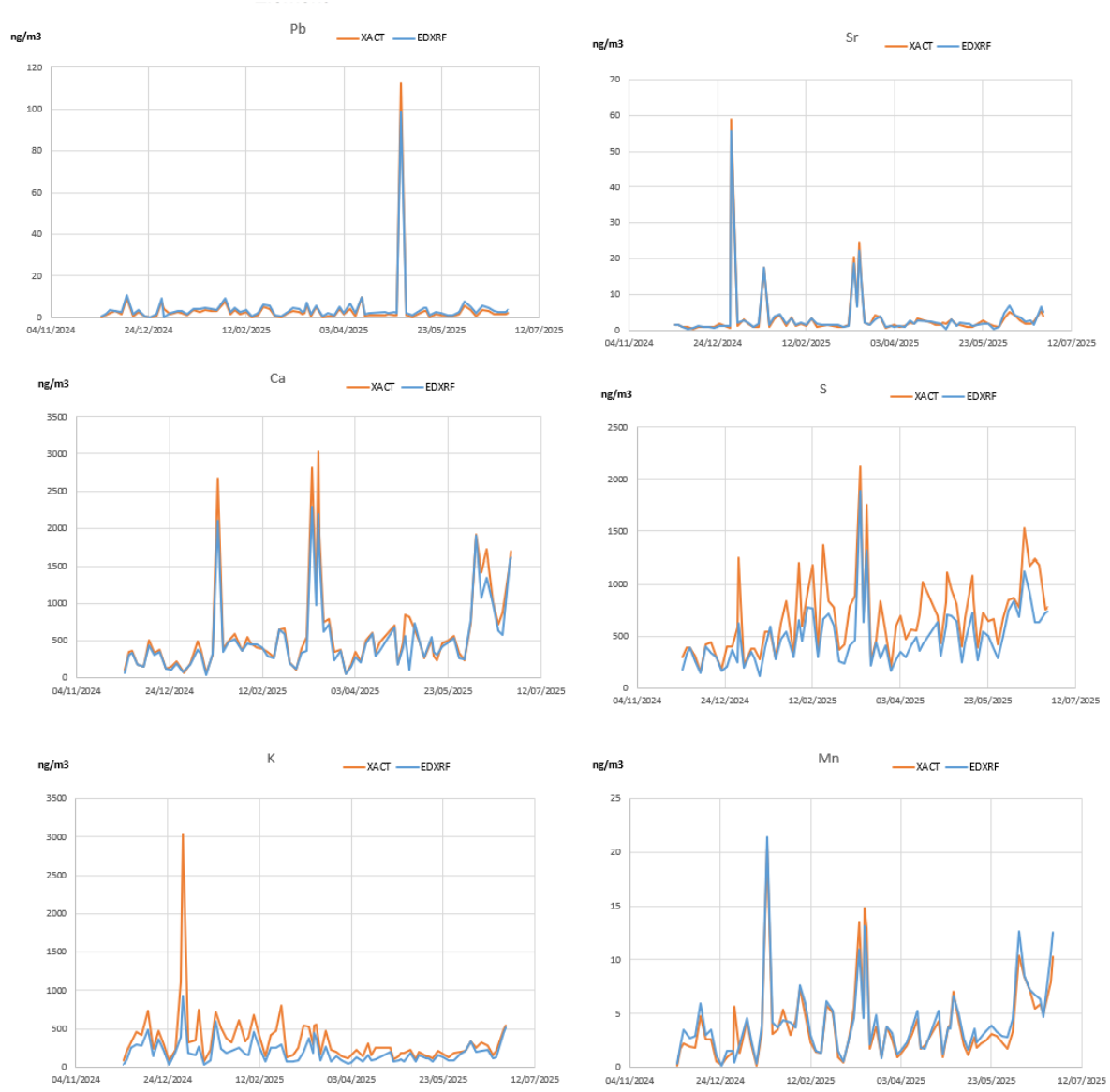

Figure 16. Some examples of daily time series of elements measured with Xact and benchtop ED-XRF for PM10.

Figure 16 shows the intercomparison time series for some specific elements suggesting that there could be an underestimation of some elements with offline ED-XRF that will be further investigated with a second step of the intercomparison in which the same filters will be analysed by both systems.

During the measurement period, 21 elements recorded at least 75% of concentrations above the LOD. These real-time measurements enhance the capability to identify and characterize atmospheric pollution sources, supporting environmental monitoring and regulatory compliance efforts. The dataset available until end of June 2025 was used to identify some characteristics of the primary emission sources impacting the ECO observatory. Figure 17 shows the average daily pattern of sulphur, silicon, calcium, and titanium, elements typically associated with crustal phenomena and secondary inorganic aerosol, which do not exhibit significant daily variability (S) or show larger values during diurnal hours (Calcium, Silicon, and Titanium).

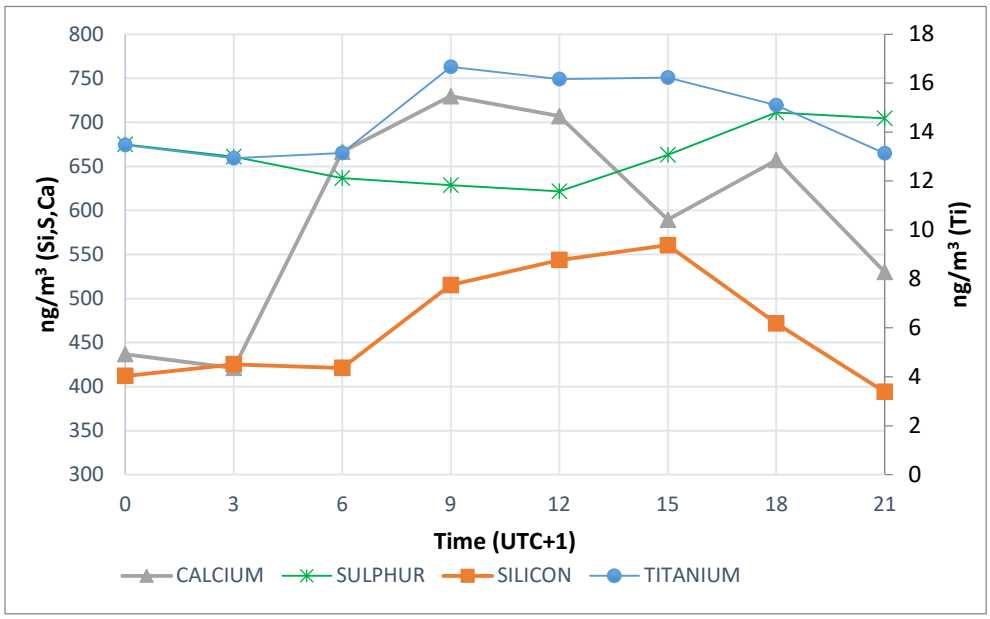

Figure 17. Average daily pattern of sulphur, silicon, calcium, and titanium.

Conversely, Figure 18 presents the daily patterns of potassium, barium, lead, and copper whose concentrations are lower during diurnal hours with a possible modulation influenced by the BLH. The daily pattern of iron, chromium, zinc, and manganese is shown in Figure 19 with concentrations fluctuating throughout the day, showing two peaks in the same period of the day in which peaks of primary organic carbon and eBC_{ff} (morning) and eBC_{bb} (night) suggesting that both combustion sources (i.e. road traffic and biomass burning) influences these elements.

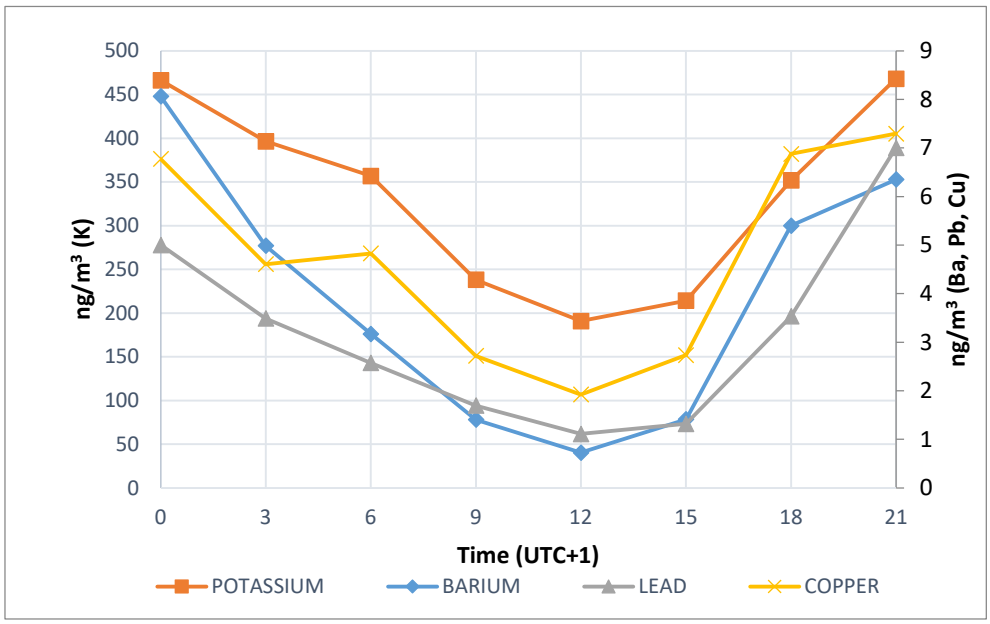

Figure 18. Average daily patterns of potassium, barium, lead, and copper.

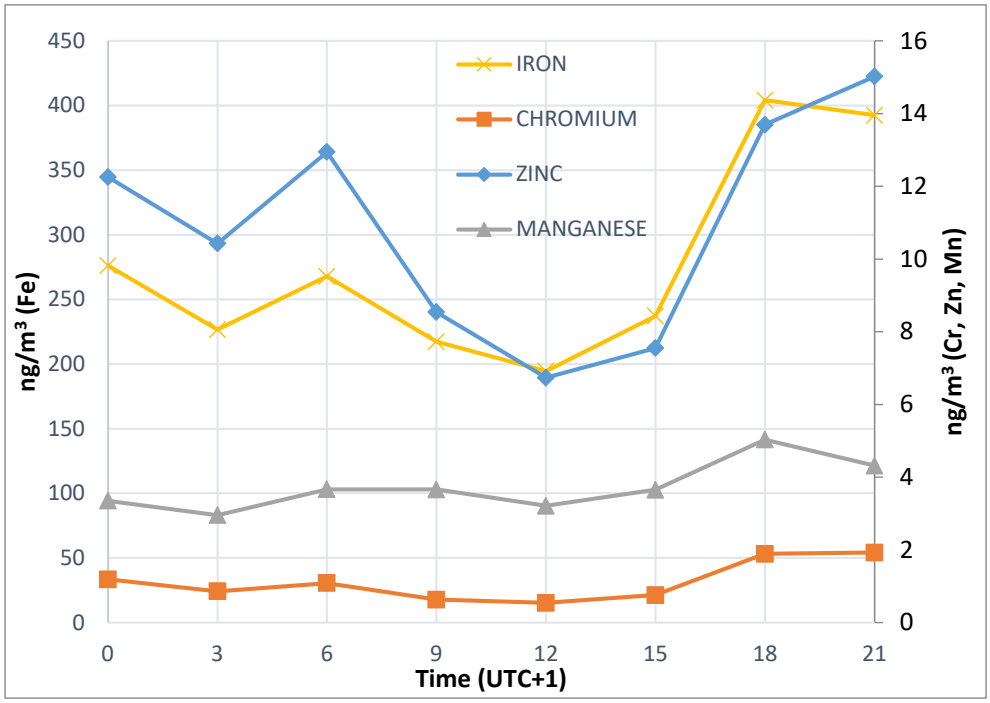

Figure 19. Average daily patterns of iron, chromium, zinc, and manganese.

Additionally, sporadic events were observed on January 1, 2025, associated with fireworks, during which peaks of typical elements such as S, Al, Ba, Bi, and Cu were recorded (see Figure 20). Many elements are used in fireworks as colour or sparkle emitters (e.g.: Al and Mg for white, Ba for green, Cu for blue, Sr for yellow) and have often been used as tracers of this source, even if they are not selective as they are also contained in soil/road dust and non-exhaust traffic emission. In the case of Bi, instead, fireworks are by far the most relevant atmospheric source of this element and its insoluble fraction constitutes a reliable and robust tracer of fireworks (Perrino et al., 2011).

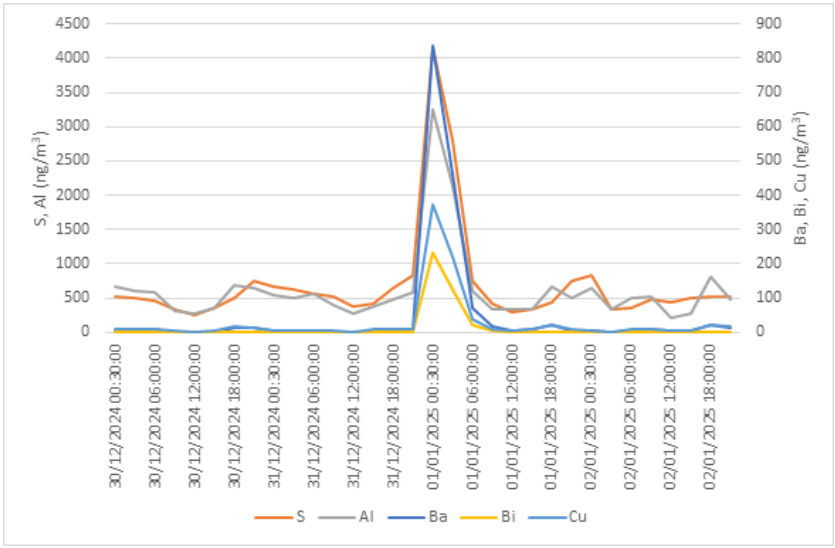

Figure 20. Peak concentrations of sulphur, aluminium, barium, and copper recorded during New Year's celebrations.

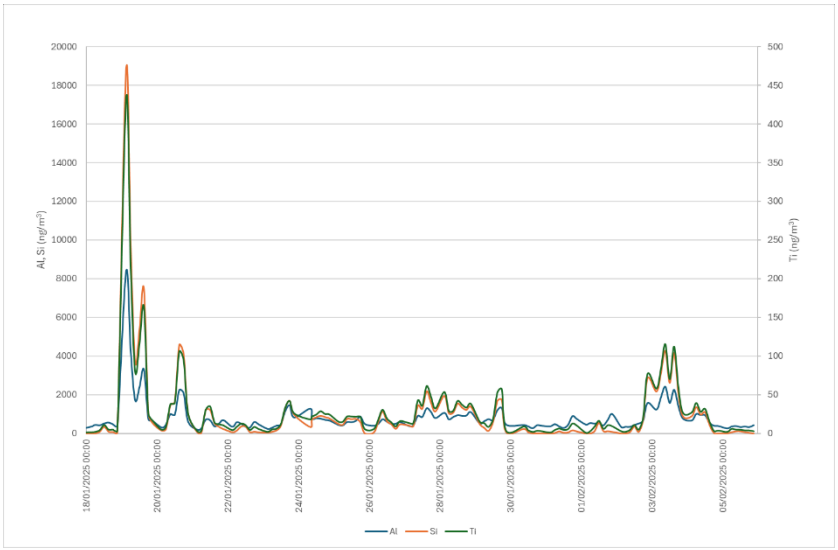

Figure 21. Silicon, aluminium, and titanium concentrations during Saharan dust events.

On January 19-20, 2025, instead, elements such as silicon, aluminium, and titanium showed correlated peaks (Figure 21), likely due to Saharan dust events. Saharan dust events have been confirmed by the dust forecasting and monitoring system developed by AEMET and the Barcelona Supercomputing Center (https://dust.aemet.es), which provides daily analyses and predictions of atmospheric dust concentrations over Europe and surrounding regions. Figure 22 presents two plots showing forecasts of Saharan dust transport towards southern Europe, with a particular impact on the Salento region (Apulia), which occurred on January 19 and February 3, 2025. The peaks on February 3 are less intense compared to the previous ones.

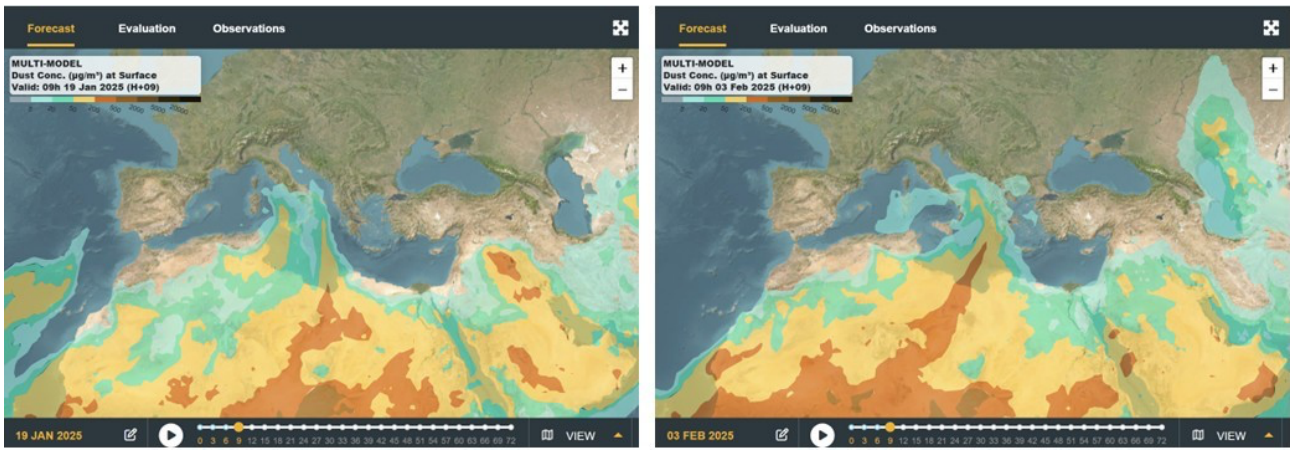

Figure 22. Atmospheric dust concentration forecasts over the Mediterranean and North African area.

CONCLUSIONS

The report shows how the new instruments for on-line measurement of aerosol composition, installed and made operative at ECO station, can be used for aerosol source identification and apportionment suggesting the potentiality of high temporal resolution in source apportionment. Future developments will include the use of receptor models applied to longer dataset at high temporal resolution combining the output of different instruments that could be the base for development of near-real-time characterization of PM sources.

REFERENCES

Bond, T.C., Habib, G., Bergstrom, R.W., 2006. Limitations in the enhancement of visible light absorption due to mixing state. J. Geophys. Res. 111, D20211.

Bond, T.C., Bergstrom, R.W., 2006. Light absorption by carbonaceous particles: an investigative review. Aerosol. Sci. Technol. 40 (1), 27-67.

Bond, T.C., Doherty, S.J., Fahey, D.W., Forster, P.M., Berntsen, T., DeAngelo, B.J., Flanner, M.G., Ghan, S., Kärcher, B., Koch, D., Kinne, S., Kondo, Y., Quinn, P.K., Sarofim, M.C., Schultz, M.G., Schulz, M., Venkataraman, C., Zhang, H., Zhang, S., Bellouin, N., Guttikunda, S.K., Hopke, P.K., Jacobson, M.Z., Kaiser, J.W., Klimont, Z., Lohmann, U., Schwarz, J.P., Shindell, D., Storelvmo, T., Warren, S.G., Zender, C.S., 2013. Bounding the role of black carbon in the climate system: a scientific assessment. J. Geophys. Res. Atmos. 118, 5380–5552.

Cesari D., Merico E., Dinoi A., Marinoni A., Bonasoni P., Contini D., 2018. Seasonal variability of carbonaceous aerosols in an urban background area in Southern Italy. Atmospheric Environment, 200, 97–108.

Cesari, D., Bloise, E., Conte, M., Dinoi, A., Deluca, G., Pennetta, A., Semeraro, P., Merico, E., Contini, D., 2025. High-Time-Resolution Measurements of Equivalent Black Carbon in an Urban Background Site of Lecce, Italy. Atmosphere 16(9), 1077.

COST Action CA16109 COLOSSAL Chemical On-Line cOmposition and Source Apportionment of fine aerosoL, Working Group 1. Guidelines for comparison of ACSM measurement with co-located external data. Deliverable 1.2. Released in December 2019. https://www.costcolossal.eu/

Daellenbach, K.R., Uzu, G., Jiang, J., Cassagnes, L.-E., Leni, Z., Vlachou, A., Stefenelli, G., Canonaco, F., Weber, S., Segers, A., Kuenen, J.J.P., Schaap, M., Favez, O., Albinet, A., Aksoyoglu, S., Dommen, J., Baltensperger, U., Geiser, M., El Haddad, I., Jaffrezo, J.-L., Prévôt, A.S.H., 2020. Sources of particulate-matter air pollution and its oxidative potential in Europe. Nature 587, 414–419.

Deluca, G., Bloise, E.; Cesari, D.; Dinoi, A.; Pennetta, A.; Potì, S.; Semeraro, P.; Unga, F.; Contini, D., 2025. Comparison of atmospheric PM10 measurements obtained by online and offline ED-XRF instrumentation. European Aerosol Conference, EAC2025.

Dinoi A., Cesari D., Marinoni A., Bonasoni P., Riccio A., Chianese E., Tirimberio G., Naccarato A., Sprovieri F., Andreoli,V., Moretti,S., Gullì D., Calidonna C.R., Ammoscato I., Contini D., 2017. Inter-comparison of carbon content in PM2.5 and PM10 collected at five measurement sites in southern Italy. Atmosphere, 8 (12), 243.

Dinoi, A., Pavese, G., Calvello, M., Chirizzi, D., Pennetta, A., De Benedetto, G. E., Esposito, F., Mapelli, C., and Contini, D.: Characterization of aerosol and its oxidative potential in a coastal semi-rural site of Southern Italy, Atmos. Environ., 333, 120656, https://doi.org/10.1016/j.atmosenv.2024.120656, 2024.

Fratticioli, C.; Wählisch, A.; Beckhoff, B.; Calzolai, G., Crazzolara, C., Chiari, M.; Giardi, F., Gross, A., Lucarelli, F., Manousakas, M.-I., Nava, S., Nowak, A., 2025. A Round Robin exercise of Xact 625i elemental analysis by intercomparison with reference-free PIXE and XRF techniques. European Aerosol Conference, EAC2025.

Kanakidou, M., Seinfeld, J.H., Pandis, S.N., Barnes, I., Dentener, F.J., Facchini, M.C., Van Dingenen, R., Ervens, B., Nenes, A., Nielsen, C.J., Swietlicki, E., Putaud, J.P., Balkanski, Y., Fuzzi, S., Horth, J., Moortgat, G.K., Winterhalter, R., Myhre, C.E.L., Tsigaridis, K., Vignati, E., Stephanou, E.G., Wilson, J., 2005. Organic aerosol and global climate modelling: A review. Atmos. Chem. Phys. 5: 1053–1123.

Ivančič M., Gregorič A., Lavrič G., Alföldy B., Ježek I., Hasheminassab S., Pakbin P., Ahangar F., Sowlat M., Boddeker S., Rigler M., 2022. Two-year-long high-time-resolution apportionment of primary and secondary carbonaceous aerosols in the Los Angeles Basin using an advanced total carbon–black carbon (TC-BC(λ)) method. Science of The Total Environment, 848, 157606.

IPCC, 2013. Climate change 2013: the physical science basis. In: Stocker, T.F., Qin, D., Plattner, G.K., Tignor, M., Allen, S.K., Boschung, J., Nauels, A., Xia, Y., Bex, V., Midgley, P.M. (Eds.), Fifth Assessment Reprot of the Intergovemental Panel on Climate Change. Cambridage University Press, Cambrigde, United Kingdom and New York, NY, USA, p. 1535.

Liu, S., Aiken, A.C., Gorkowski, K., Dubey, M.K., Cappa, C.D., Williams, L.R., Herndon, S.C., Massoli, P., Fortner, E.C., Chhabra, P. S., Brooks, W. A., Onasch, T. B., Jayne, J.T., Worsnop, D.R., China, S., Sharma, N., Mazzoleni, C., Xu, L., Ng, N.L., Liu, D., Allan, J.D., Lee, J.D., Fleming, Z.L., Mohr, C., Zotter, P., Szidat, S., and Prévôt, A.S.H., 2015. Enhanced light absorption by mixed source black and brown carbon particles in UK winter. Nat. Commun. 6, 8435.

Massabò D., Prati P., 2021. An overview of optical and thermal methods for the characterization of carbonaceous aerosol. La Rivista del Nuovo Cimento (2021) 44:145–192.

Merico, E., Cesari, D., Dinoi, A., Potì, S., Pennetta, A., Bloise, E., Contini, D., in press. Long-term analysis of carbonaceous fractions of particulate at a Central Mediterranean site in Italy. Atmos. Poll. Res. 2025, (11) 16, 102668.

Perrino, C., Tiwari, S., Catrambone, M., Dalla Torre, S., Rantica, E., & Canepari, S. (2011). Chemical characterisation of atmospheric PM in Delhi, India, during different periods of the year including Diwali festival. Atmospheric Pollution Research, 2(4), 418-427.

Putaud, J.P., Van Dingenen, R., Alastuey, A., Bauer, H., Birmili, W., Cyrys, J., Flentje, H., Fuzzi, S., Gehrig, R., Hansson, H.C., Harrison, R.M., Herrmannd, H., Hitzenberger, R., Hüglin, C., Jones, A.M., Kasper-Giebl, A., Kiss, G., Kousa, A., Raesa, F., 2010. A European aerosol phenomenology 3: Physical and chemical characteristics of particulate matter from 60 rural, urban, and kerbside sites across Europe. Atmos. Environ. 44: 1308–1320.

Sandradewi, J., Prevot, A. S. H., Szidat, S., Perron, N., Alfarra, M. R., Lanz, V. A., Weingartner, E., and Baltensperger, U. Using aerosol light absorption measurements for the quantitative determination of wood burning and traffic emission contributions to particulate matter, Environ. Sci. Technol. 2008, 42, 3316–3323.

Tomašek, I., Damby, D.E., Andronico, D., Baxter, P.J., Boonen, I., Claeys, P., Denison, M.S., Horwell, C.J., Kervyn, M., Kueppers, U., Romanias, M.N., Elskens, M., 2021. Assessing the biological reactivity of organic compounds on volcanic ash: implica- tions for human health hazard. Bull. Volcanol. 83, 30.

Unga, F., Calzolai, G., Chiari, M., Cuccia, E., Colombi, C., Franciosa, M., Dinoi, A., Merico, E., Pennetta, A., Gómez-Sánchez, N., Mapelli, C., Pareti, S., Perrino, C., Yubero, E., and Contini, D.,

2025. Determination of aerosol composition by ED-XRF on Teflon and quartz substrates: potentialities and limits, Aerosol Research, 3, 405–415, https://doi.org/10.5194/ar-3-405-2025.

WHO, 2021. WHO Global Air Quality Guidelines: Particulate Matter (PM2.5 and PM10), Ozone, Nitrogen Dioxide, Sulfur Dioxide and Carbon Monoxide. World Health Organization.

Zotter, P., Herich, H., Gysel, M., El-Haddad, I., Zhang, Y., Močnik, G., Hüglin, C., Baltensperger, U., Szidat, S., and Prévôt, A. S. H. Evaluation of the absorption Ångström exponents for traffic and wood burning in the Aethalometer-based source apportionment using radiocarbon measurements of ambient aerosol. Atmos. Chem. Phys. 2017, 17, 4229–4249, https://doi.org/10.5194/acp-17-4229-2017.